JACS
JOURNAL OF THE AMERICAN CHEMICAL SOCIETY
Article
pubs.acs.org/JACS

Highly Active and Stable Hybrid Catalyst of Cobalt-Doped FeS_2 Nanosheets–Carbon Nanotubes for Hydrogen Evolution Reaction

Di-Yan Wang,[†,‡,§] Ming Gong,[†] Hung-Lung Chou,[∥] Chun-Jern Pan,[⊥] Hsin-An Chen,[#] Yingpeng Wu,[†] Meng-Chang Lin,[†] Mingyun Guan,[†] Jiang Yang,[†] Chun-Wei Chen,[#] Yuh-Lin Wang,[§] Bing-Joe Hwang,*[,⊥] Chia-Chun Chen,*[,‡,§] and Hongjie Dai*[,†]

[†]Department of Chemistry, Stanford University, Stanford, California 94305, United States
[‡]Department of Chemistry, National Taiwan Normal University, Taipei 11677, Taiwan
[§]Institute of Atomic and Molecular Science, Academia Sinica, Taipei 10617, Taiwan
[∥]Graduate Institute of Applied Science and Technology, National Taiwan University of Science and Technology, Taipei 10607, Taiwan
[⊥]Department of Chemical Engineering, National Taiwan University of Science and Technology, Taipei 10607, Taiwan
[#]Department of Materials Science and Engineering, National Taiwan University, Taipei 10617, Taiwan

Supporting Information

ABSTRACT: Hydrogen evolution reaction (HER) from water through electrocatalysis using cost-effective materials to replace precious Pt catalysts holds great promise for clean energy technologies. In this work we developed a highly active and stable catalyst containing Co doped earth abundant iron pyrite FeS_2 nanosheets hybridized with carbon nanotubes ($Fe_{1-x}Co_xS_2$/CNT hybrid catalysts) for HER in acidic solutions. The pyrite phase of $Fe_{1-x}Co_xS_2$/CNT was characterized by powder X-ray diffraction and absorption spectroscopy. Electrochemical measurements showed a low overpotential of ~0.12 V at 20 mA/cm^2, small Tafel slope of ~46 mV/decade, and long-term durability over 40 h of HER operation using bulk quantities of $Fe_{0.9}Co_{0.1}S_2$/CNT hybrid catalysts at high loadings (~7 mg/cm^2). Density functional theory calculation revealed that the origin of high catalytic activity stemmed from a large reduction of the kinetic energy barrier of H atom adsorption on FeS_2 surface upon Co doping in the iron pyrite structure. It is also found that the high HER catalytic activity of $Fe_{0.9}Co_{0.1}S_2$ hinges on the hybridization with CNTs to impart strong heteroatomic interactions between CNT and $Fe_{0.9}Co_{0.1}S_2$. This work produces the most active HER catalyst based on iron pyrite, suggesting a scalable, low cost, and highly efficient catalyst for hydrogen generation.

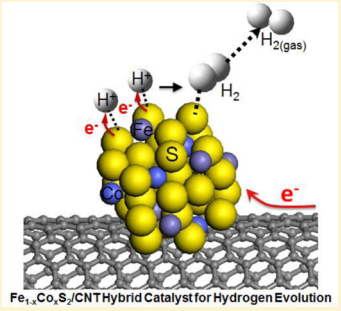

1. INTRODUCTION

Hydrogen could be an economic fuel used in electrochemical cell for powering vehicles or electric devices. Producing hydrogen fuel has attracted intense search for effective electrocatalysts for the hydrogen evolution reaction (HER).[1−5] Recently, researchers have investigated the possibility of using earth abundant and inexpensive binary metal sulfide,[6−13] nitride,[14] boride,[15] and phosphide[16] to replace precious metal Pt as HER electrocatalysts. For hydrogenase systems in nature, metal sulfur clusters with five permanent ligands in a distorted octahedral ligation shell have been proven to be the active sites for HER.[17] Many efforts have been taken to synthesize inorganic metal sulfur complexes and solids to create analogous mimics of the active site. For example, MoS_2 nanostructures supported on Au,[6] graphene,[18] and carbon materials[19,20] have been demonstrated to exhibit high HER catalytic activity due to active edges of MoS_2 surface. Other transition metal sulfides of tungsten, cobalt,[10−12] nickel,[10] and iron[10,13] were also reported to be catalytically active for HER. Nevertheless, much remains to be done to understand the catalytic activity and improve catalyst synthesis.

Doping metal catalysts with additional metal atoms is an important approach to enhance the activity of electrocatalysts. In the past two decades, platinum metal alloyed with transition metal has been demonstrated to be more efficient than pure platinum in methanol oxidation reaction (MOR) and oxygen reduction reaction (ORR).[21−24] Previous spectroscopic and theoretical studies indicated that the enhancement of MOR and ORR activity was attributed to the increase of charge transfer from transition metal atoms to platinum, resulting in weaker bonding of CO molecule and O_2 molecule adsorbed on Pt, respectively.[25,26] In HER, the catalytic capability exhibited a strong dependence on the hydrogen adsorption energy and kinetic energy barrier of hydrogen evolution pathway, which could be varied by the type of atom or crystal phase exposed on the surface of catalysts.[27] Some studies demonstrated that HER

Received: November 11, 2014
Published: January 14, 2015

DOI: 10.1021/ja511572q
J. Am. Chem. Soc. 2015, 137, 1587−1592

activity of metal sulfide was improved by doping other transition metal but still was not good enough.[10,13] In the [Fe−Ni] hydrogenase case, theoretical calculation indicated that the system fulfills the optimal hydrogen adsorption energy condition of ∼0 eV.[28,29] Therefore, modifying the electronic structure of metal sulfide materials by doping metal atoms could be a key to optimize hydrogen adsorption energy and enhance HER catalytic activity.

To date, the investigation of 3d transition metal chalcogenides as HER electrocatalyst is still limited. Some reports have demonstrated that metal chalcogenide thin films were grown on glassy carbon or fluorine doped tin oxide electrode and showed good electrocatalytic activity for HER.[12,13] Rational design of low-cost bulk quantities of iron pyrite composites as large scale HER catalysts could lead to a new series of catalytic materials for practical use. Although the intrinsic conductivity of bulk iron pyrite is quite high (1 S/cm),[30] iron pyrite nanocrystal thin film has low conductivity (10^{-4} S/cm), which is critical to the electrocatalytic performance.[31] Our recent studies have demonstrated that the hybridization of the catalysts with nanocarbon materials such as carbon nanotube and graphene can lead to reduced overpotential and improved stability in electrocatalysis.[32−37] The enhancement of electrocatalytic performance was attributed to increased surface area, enhanced charge transport, and strong chemical bonding between inorganic electrocatalysts and nanocarbon materials.

Here, we report scalable synthesis of highly active and stable Co-doped iron pyrite (FeS_2) electrocatalysts on carbon nanotube ($Fe_{1-x}Co_xS_2$/CNT) hybrid catalysts for HER. We found that the electrocatalytic activities of $Fe_{1-x}Co_xS_2$/CNT hybrid catalysts are strongly related to Co doping ratio. The $Fe_{0.9}Co_{0.1}S_2$/CNT hybrid catalyst achieved the lowest overpotential of ∼0.12 V at 20 mA/cm^2, a Tafel slope of ∼46 mV/decade, and excellent stability over 40 h in acid condition. Density functional theory (DFT) calculation revealed that sulfur in $Fe_{0.9}Co_{0.1}S_2$ structure was responsible for the active sites for proton adsorption and reduction. The detailed reaction kinetic pathway and hydrogen adsorption energy of $Fe_{0.9}Co_{0.1}S_2$ for HER catalysis were also elucidated.

2. EXPERIMENTAL SECTION

Preparation of Oxidized Multiwalled Carbon Nanotubes (MWCNTs). MWCNTs (FloTube 9000, CNano Technology Ltd.) were oxidized by a modified Hummers method.[38] A 1 g portion of MWCNTs was purified by annealing process at 500 °C and washing with 40 mL of diluted hydrochloric acid (10 wt %) to remove metal residues and amorphous carbon. The purified MWCNTs were repeatedly washed with water and then collected. After drying overnight, ∼23 mL of concentrated sulfuric acid was mixed with the purified MWCNTs (∼0.99 g) in a 250 mL round flask and stirred at room temperature for 12 h. Subsequently, the round flask was heated to 40 °C in an oil bath, followed by slow addition of ∼100 mg of $NaNO_3$ (99%, Sigma-Aldrich) and ∼1 g of $KMnO_4$ (99%, Sigma-Aldrich) (about the same as the mass of purified MWCNTs). After stirring at 40 °C for 30 min, 3 mL of water was added, followed by another 3 mL after 5 min. A 40 mL portion of water was slowly added 5 min later to keep the temperature below 45 °C. After 15 min, 140 mL of water was poured into the solution at room temperature, followed by addition of 10 mL of 30% H_2O_2 to stop the reaction after 10 min. The 1× oxidized MWCNTs were collected, washed with diluted HCl solution (5 wt %) twice, and then water repeatedly until pH is higher than or equal to 5. The final suspension (in H_2O) was lyophilized to get solid oxidized MWCNTs. The 2× and 4.5× oxidized MWCNTs were also following the above-mentioned procedures with adjusting the additional weight of $KMnO_4$ to 2 and 4.5 times in comparison with the weight of MWCNTs, respectively.

Preparation of $Fe_{1-x}Co_xS_2$/CNT Hybrid Catalysts. In a typical synthesis of $Fe_1Co_0S_2$/CNT, $Fe_{0.95}Co_{0.05}S_2$/CNT, $Fe_{0.9}Co_{0.1}S_2$/CNT, $Fe_{0.66}Co_{0.34}S_2$/CNT, and $Fe_{0.37}Co_{0.63}S_2$/CNT hybrid catalysts, ∼4 mg of oxidized MWCNTs was sonicated in 8 mL of anhydrous *N*,*N*-dimethylformamide (DMF) (99.8%, Acros) for 10 min, followed by addition of 0.8 mL of 0.2 M iron nitrite ($Fe(NO_3)_3$) (99%, Acros), 2 mL of 1 M thioacetamide (TAA) (99%, Sigma-Aldrich), and 0, 0.04, 0.08, 0.16, and 0.4 mL of 0.2 M cobalt acetate ($Co(Ac)_2$) (>98%, Sigma-Aldrich) aqueous solution, respectively. The mixture was vigorously stirred at 90 °C in an oil bath for 24 h. The suspension was centrifuged and washed with H_2O twice to remove residue with no reacting, and then the precipitant was obtained. The precipitant was redissolved into 8 mL of DMF. The suspension was heated to and maintained at 180 °C for 5 h in an autoclave. After cooling down to room temperature, the sample was collected, centrifuged, washed with water, and finally lyophilized to get solid $Fe_{1-x}Co_xS_2$/CNT hybrid catalysts.

Materials Characterizations. Transmission electron microscopy (TEM) and electron energy loss spectroscopy (EELS) mapping were performed on a Philips Technai G2 (FEI-TEM) microscope operating at 200 kV. The samples for the TEM analysis were prepared by ultrasonically dispersing the hybrid materials in ethanol. XPS spectra were recorded on a PHI 5000 VersaProbe system (ULVAC-PHI, Chigasaki, Japan) using a microfocused (100 μm, 25 W) Al Kα X-ray with a photoelectron takeoff angle of 45° and a 23.5 eV pass energy. A drop of the suspension was applied onto a lacey carbon-coated copper grid and then dried in air. Hard X-ray absorption spectroscopy (XAS) spectra were collected at the beamline BL17C at National Synchrotron Radiation Research Center (NSRRC), Hsinchu, Taiwan. The storage ring of the electronic accelerator can supply the electronic energy of 1.5 GeV and the current operating at 360 mA. A Si(111) double crystal monochromator was used to perform energy scan, of which the parallelism can be adjusted to eliminate the high order harmonics. All XAS data were recorded using the transmission mode. The ionization chambers were applied as detectors to monitor the intensity of the incident and transmitted beams through the specimen. The absorption coefficient can be calculated from the logarithm of the intensity ratio of the incident and transmitted beams. The reference Fe and Co metal foils were positioned in front of the window of the third ionization chamber and measured simultaneously as a standard for energy calibration in each energy scan. The beam size was limited by the horizontal and vertical slits with the area of 2 × 2 mm^2 during XAS measurements.

Preparation of Sample for Electrochemical Measurement. To prepare the $Fe_{1-x}Co_xS_2$/CNT hybrids on RDE electrode, 1 mg of hybrid was mixed with 190 μL of water, 50 μL of ethanol, and 10 μL of 5 wt % Nafion solution by at least 30 min sonication to form a homogeneous ink. Subsequently, 20 μL of suspension was drop-dried onto a glassy carbon electrode of 5 mm in diameter (loading of 0.40 mg/cm^2, including CNTs). To prepare the hybrid materials on Ti foil electrode, hybrid was dispersed in ∼2 mL ethanol with 3 wt % PTFE (from its 60 wt % water suspension, Aldrich). After sonication for 10 min, all suspension was drop-dried onto 1 cm × 1 cm Ti foil at 90 °C. The electrode was further heated at 120 °C for ∼20 min until fully dry.

Electrochemical Measurement. HER catalytic activity measurement was performed in a standard three-electrode system controlled by a CHI 760D electrochemistry workstation. Catalyst powders cast on RDE or Ti foil were used as working electrode, graphite rod as counter electrode, and saturated calomel electrode as reference electrode. The reference was calibrated against and converted to reversible hydrogen electrode (RHE). RDE electrode was constantly rotating at 1600 rpm to get rid of the bubbles during the measurement. Linear sweep voltammetry was carried out at 1 mV/s for the polarization curves. Chronopotentiometry was measured under a constant current density of 20 mA/cm^2. All polarization curves were *i*R-corrected. The electrolyte was 0.5 M H_2SO_4, which has constant pH of 0 over the course of the experiment. In addition, to estimate the faraday yield, the hydrogen gas was collected by a microsyringes (1

DOI: 10.1021/ja511572q
J. Am. Chem. Soc. 2015, 137, 1587−1592

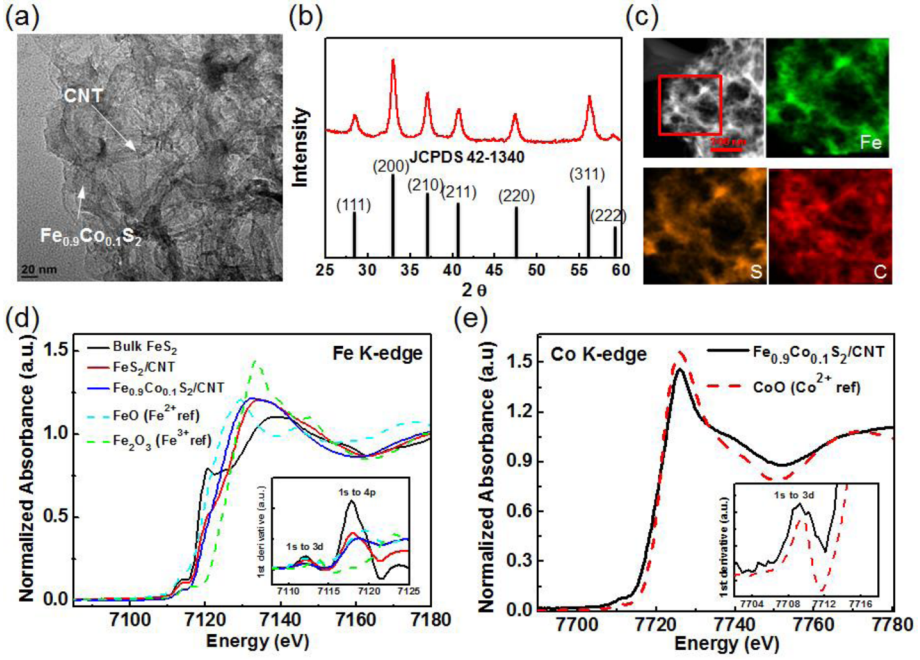

Figure 1. (a) HRTEM image and (b) XRD pattern of $Fe_{0.9}Co_{0.1}S_2$/CNT hybrid catalyst. (c) HAADF-STEM images and EDS mapping of $Fe_{0.9}Co_{0.1}S_2$/CNT hybrid catalyst. (d) Normalized XANES spectra near Fe K-edge of the hybrid catalysts and Fe references. (e) Normalized XANES spectra near Co K-edge of hybrid catalysts and Co reference. The Fe and Co K-pre-edges of the hybrid catalysts were shown in the inset of parts d and e, respectively.

mL) and measured under ex-situ gas chromatography with TCD detector.

3. RESULTS AND DISCUSSION

Synthesis and Characterization of $Fe_{1-x}Co_xS_2$/CNT Hybrid Catalysts. A series of $Fe_{1-x}Co_xS_2$/CNT hybrid catalysts were synthesized by a low-temperature solution-phase reaction of iron nitrate, cobalt acetate, and thioacetamide in *N*,*N*-dimethylformamide (DMF) suspension of mildly oxidized carbon nanotubes (CNT), followed by a high-temperature solvothermal process for crystallization of $Fe_{1-x}Co_xS_2$ catalysts and reduction of CNT. We investigated the morphology, structure, and composition of representative $Fe_{0.9}Co_{0.1}S_2$/CNT hybrid catalyst (Figure 1). High-resolution transmission electron microscopy (HRTEM, Figure 1a) revealed that the $Fe_{0.9}Co_{0.1}S_2$ catalyst exhibited nanosheet morphology interconnected with CNT. Scanning electron microscopy (SEM) images confirmed a two-dimensional sheet-like morphology (Supporting Information Figure S1). X-ray photoelectron spectroscopy (XPS) analysis of the $Fe_{0.9}Co_{0.1}S_2$/CNT hybrid catalyst exhibited an elemental composition of Fe:Co:S close to 0.9:0.1:2 (see Supporting Information). Powder X-ray diffraction pattern (Figure 1b) of $Fe_{0.9}Co_{0.1}S_2$/CNT hybrid catalyst was consistent with a FeS_2 pyrite standard pattern (JCPDS no. 42-1340) with planes indexed to the (111), (200), (210), (211), (220), (311), and (222) planes, respectively.

To further glean the structure of $Fe_{0.9}Co_{0.1}S_2$/CNT hybrid catalyst, high-angle annular dark-field scanning TEM (HAADF-STEM) and selected area EDX mapping were performed, revealing a homogeneous distribution of Fe, S, and C in the catalyst (Figure 1c). X-ray adsorption spectroscopy (XAS) of $Fe_{0.9}Co_{0.1}S_2$/CNT was performed to investigate the Fe and Co bonding environment. Fe K-edge and Co K-edge X-ray adsorption near-edge spectra (XANES) were obtained (Figure 1d,e, respectively). By measuring the edge jump ($\Delta\mu$) in XANES spectra, we estimated a Fe/Co molar ratio ~0.9/0.1, consistent with XPS result. The first derivatives of the Fe and Co K-pre-edges (representing the electronic transitions from 1s core level to unoccupied 3d or 4p, see inset of Figure 1d,e, respectively) were close to the references of FeO (Fe^{2+}) and CoO (Co^{2+}), suggesting that the oxidation states of both Fe and Co were +2 in the $Fe_{0.9}Co_{0.1}S_2$/CNT hybrid catalyst. The bonding environment of Co atoms was investigated by Fourier transformed k^3-weighted extended X-ray absorption fine structure spectra (EXAFS) at Co edge for the $Fe_{0.9}Co_{0.1}S_2$/CNT hybrid catalyst. The results showed that only Co−Fe and Co−S bonding but no Co−Co bonding was found and their coordination numbers were estimated to be ~5.6 and ~5.1, respectively (Supporting Information Table S1). The presence of Co−Fe bonding with bond distance of 3.85 Å indicated that Co atoms were successfully doped into the crystal structure of iron pyrite without phase separation. The coordination numbers of Fe−Fe, Fe−Co, and Co−Fe bonding for $Fe_{0.9}Co_{0.1}S_2$/CNT hybrid catalyst are less than 12 for a bulk iron pyrite material,[39] indicating the catalyst with nanodomains formed from the synthesis process. When the Co content was increased to 0.34 and 0.64 (from XANES of Co-edge in Supporting Information Figure S3b), formation of cobalt sulfide with pentlandite structure was observed, suggesting phase separation in the hybrid catalysts[40] likely related to lower HER activity of the hybrid catalyst with higher Co content.

Hydrogen Evolution Reaction Activity of $Fe_{1-x}Co_xS_2$/CNT Hybrid Catalysts. Figure 2a showed that the HER activities of $Fe_{1-x}Co_xS_2$/CNT hybrid catalysts were evaluated under acidic conditions (0.5 M H_2SO_4) in a typical three-electrode configuration to compare with a commercial Pt/C catalyst (Fuel Cell Store, 20 wt %). For $Fe_{1-x}Co_xS_2$/CNT catalysts (x = 0, 0.05, 0.1 0.34, and 0.63, measured by X-ray absorption spectra), an optimal HER catalytic activity was

DOI: 10.1021/ja511572q
J. Am. Chem. Soc. 2015, 137, 1587−1592

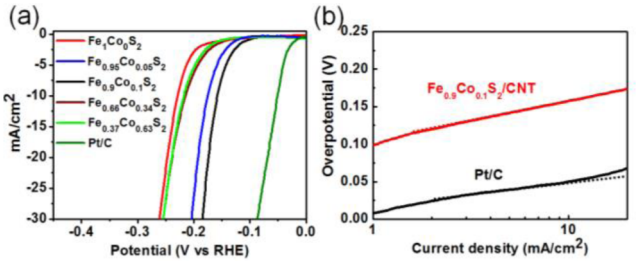

Figure 2. (a) Polarization curves obtained with a series of $Fe_{1-x}Co_xS_2$/CNT hybrid catalysts as indicated and (b) corresponding Tafel plots recorded on glassy carbon electrodes with $Fe_{0.9}Co_{0.1}S_2$/CNT hybrid catalyst and Pt/C catalyst loading of 0.4 mg/cm^2 (including the mass of CNT (~30 wt %)). Each dashed line is the fitting slope of the corresponding Tafel plot.

obtained when x = 0.1 with the lowest onset potential (~0.09 V) and a rapid cathodic current increase at high biases (Figure 2a). Increasing or decreasing Co doping ratio (compared to x = 0.1) led to lower activity of the $Fe_xCo_{1-x}S_2$/CNT hybrid catalysts. In comparison, Pt/C afforded onset potential of near 0 V for HER catalysis. The linear parts of the Tafel plots (Figure 2b) revealed Tafel slopes of ~30 and ~46 mV/decade for Pt/C and $Fe_{0.9}Co_{0.1}S_2$/CNT hybrid catalyst, respectively. The ~46 mV/decade Tafel slope of $Fe_{0.9}Co_{0.1}S_2$/CNT hybrid catalyst was the smallest measured to date for FeS_2 catalysts.[13]

Activity and Stability of Hybrid Catalysts for HER. Catalyst stability was investigated by continuous cyclic voltammetry (CV) on glassy carbon substrate in the voltage range of 0 and −0.4 V versus RHE at a constant scanning rate of 50 mV/s over 1000 cycles without *iR* compensation (Figure 3a). No change in the polarization curve of $Fe_{0.9}Co_{0.1}S_2$/CNT hybrid catalyst after 1000 cycles was observed, suggesting stable HER electrocatalysis of the material in acid. Toward practical electrolyzers, we investigated HER performance of our $Fe_{0.9}Co_{0.1}S_2$/CNT hybrid catalyst under high loadings onto

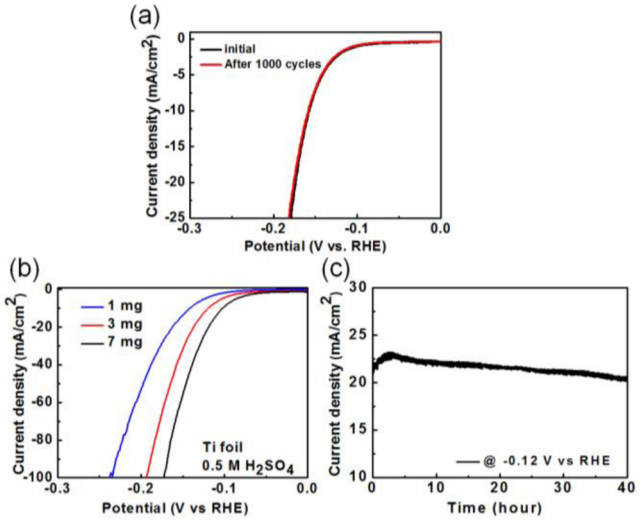

Figure 3. (a) Stability test for HER of the $Fe_{0.9}Co_{0.1}S_2$/CNT hybrid catalyst. Negligible HER current was lost after 1000 cycles. (b) Polarization curves recorded on Ti foil with high amount loading of 1, 3, and 7 mg/cm^2 (including the mass of CNT (~30 wt %)). (c) Current versus time during the long term (40 h) with a constant potential (−0.12 V) electrolysis of $Fe_{0.9}Co_{0.1}S_2$/CNT hybrid catalysts on Ti foil with loading of 7 mg/cm^2.

titanium foils. The $Fe_{0.9}Co_{0.1}S_2$/CNT hybrid catalyst loaded up to 7 mg/cm^2 (including the mass of CNT (~30 wt %)) on Ti foil could achieve high HER current densities of 20 and 100 mA/cm^2 at low overpotentials of 0.12 and 0.17 V, respectively (Figure 3b). To calculate the turnover frequency (TOF) of the $Fe_{0.9}Co_{0.1}S_2$/CNT hybrid catalyst, we measured the surface area of our hybrid material to be ~80.1 m^2 g^{-1} by Brunauer–Emmett–Teller (BET) measurement. On the basis of the surface area, the turnover frequency (TOF) was calculated to be 0.31 s^{-1} at an overpotential of 170 mV, assuming all the surface sulfur sites were participating in the HER catalysis (see Supporting Information for detailed calculations). Also, the Faraday yield of hydrogen production was then calculated. The yield was almost over 99% during 10 min of electrolysis (see Supporting Information Figure S12). In addition, $Fe_{0.9}Co_{0.1}S_2$/CNT hybrid catalyst was able to maintain a stable HER current density at ~20 mA/cm^2 for ~40 h at a constant voltage of −0.12 V versus RHE in 0.5 M H_2SO_4 (Figure 3c). With the excellent activity, stability, cost-effectiveness, and corrosion-resistance, the $Fe_{0.9}Co_{0.1}S_2$/CNT hybrid catalyst holds promise as a new HER catalyst to replace precious Pt catalyst for various applications such as PEM water electrolysis.

Role of Carbon Nanotube of Electrocatalytic Activity Enhancement: Electrical Conductivity. To study the catalytic activity of hybrid catalysts affected by conductivity of CNT, samples of $Fe_{0.9}Co_{0.1}S_2$ hybridized with CNT with different oxidation degrees (1×CNT, 2×CNT, and 4.5×CNT, by using different $KMnO_4$ oxidizer to C mass ratios of 1, 2, 4.5 in a modified Hummers method, respectively, see Supporting Information for details) were obtained. Figure 4a showed that

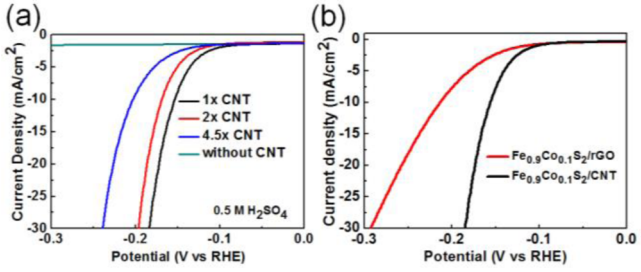

Figure 4. (a) Polarization curve obtained with the $Fe_{0.9}Co_{0.1}S_2$/CNT with different oxidation degrees (1×CNT, 2×CNT, and 4.5×CNT). (b) Polarization curve obtained with the $Fe_{0.9}Co_{0.1}S_2$/CNT and $Fe_{0.9}Co_{0.1}S_2$/rGO hybrid catalysts.

$Fe_{0.9}Co_{0.1}S_2$/CNT (1×: lowest oxidation degree) hybrid catalyst exhibited the best HER catalytic activity. With the increase of oxidation degree of CNT, the hybrid catalysts resulted in lower HER catalytic activity of the final product, due to that excessive oxidation destroyed the electrical conductivity of nanotubes desired for electrocatalysis according to Nyquist plot analysis (see Supporting Information Figure S10).[33] For comparison, the $Fe_{0.9}Co_{0.1}S_2$ with no CNTs prepared under identical synthesis condition exhibited very low HER catalytic activity. The synthesis of $Fe_{0.9}Co_{0.1}S_2$ with no CNT afforded nanoparticle morphology (see Supporting Information Figure S6) instead of nanosheet on CNTs, suggesting the mildly oxidized CNTs served as nucleation and growth substrate for $Fe_{0.9}Co_{0.1}S_2$ and in turn affected the growth morphology. The sheet-like morphology provided abundant edges that could serve as active sites for HER catalysis, as in the case of MoS_2 and WS_2.[6,7,41,42]

DOI: 10.1021/ja511572q
J. Am. Chem. Soc. 2015, 137, 1587–1592

The catalytic activities of the $Fe_{0.9}Co_{0.1}S_2$/reduced graphene oxide (rGO) hybrid catalysts prepared under solvothermal synthetic process (see Supporting Information) were measured in comparison with that of $Fe_{0.9}Co_{0.1}S_2$/CNT hybrid catalysts as shown in Figure 4b. We found that the HER activity of $Fe_{0.9}Co_{0.1}S_2$/CNT hybrid catalysts was much better than that of $Fe_{0.9}Co_{0.1}S_2$/rGO hybrid catalysts. These results suggested that the enhancement of electrocatalytic HER activity strongly depended on the nanocarbon materials used for the hybrid catalysts.[43,44] Our previous studies indicated that that nonprecious Co_3O_4–N doped reduced graphene hybrid catalyst exhibited high ORR electrochemical performance due to the formation of interfacial covalent Co–O–C and Co–N–C bonds in the Co_3O_4–graphene hybrid.[45] Bond formation between inorganic nanocatalysts and the underlying carbon support could change the chemical bonding environment for carbon, oxygen, and metal atoms in the hybrid material, resulting in enhancing catalytic activity. Overall, our results suggested that the advantages of hybrids of multiwalled CNT and $Fe_{0.9}Co_{0.1}S_2$ are the ability of mildly oxidizing the outer walls of nanotubes for generating abundant functional groups and defects needed for nucleation and growth of nanoparticles while maintaining sufficiently high electrical conductivity of nanotubes through the relatively undamaged inner tubes.

Role of Cobalt-Doping of Electrocatalytic Activity Enhancement: DFT Calculation. To understand the Co doping effect on catalytic activity of iron pyrite-CNT for HER, we investigated the detailed HER pathways on the FeS_2–CNT and $Fe_{0.9}Co_{0.1}S_2$–CNT catalysts by DFT calculations (see Supporting Information for calculation details). The reaction pathway in acid solution mainly involved proton adsorption and reduction on the catalyst surface to form hydrogen atom adsorbed on catalyst edge, followed by H_2 formation and desorption on the catalyst edge (Figure 5a).[19,27] Through DFT calculation, the sulfur atom on the edge of iron pyrite catalyst was found to be the HER active site (see Supporting Information). Both FeS_2–CNT and $Fe_{0.9}Co_{0.1}S_2$–CNT surfaces showed only slightly higher hydrogen adsorption energy (E_H) and similar hydrogen molecule adsorption energy (E_{H2}) compared to Pt (111) surface (Figure 5b), demonstrating the highly active nature of iron pyrite catalysts in stabilizing HER intermediate and releasing H_2 gas.

According to previous reports, the HER activity of platinum catalysts is also related to the kinetic energy barrier of hydrogen evolution pathway.[29,46] To understand the mechanism of improved activity by Co incorporation, we further investigated the kinetic energy barrier profiles of HER on FeS_2–CNT and $Fe_{0.9}Co_{0.1}S_2$–CNT slabs by DFT (Figure 5c). The energy barrier for transition state 1 (TS1) of hydrogen atom adsorption (H_{ads} + H_{ads}) on the $Fe_{0.9}Co_{0.1}S_2$–CNT slab was found to be 1.23 eV, which was significantly lower than that on FeS_2–CNT (1.62 eV). The bond length of H–S on S site of FeS_2–CNT (110) was also estimated to 1.361 Å, shorter than 1.365 Å on the S site of $Fe_{0.9}Co_{0.1}S_2$–CNT (110) (see Supporting Information). The longer bond length of H–S on $Fe_{0.9}Co_{0.1}S_2$–CNT (110) created a situation in which the sulfur–hydrogen bonds on Co-doped iron pyrite were weakened such that a hydrogen atom could approach the active site to form a H–H bond more effectively. Overall, iron pyrite catalysts exhibited suitable adsorption energy for H_2 evolution, and Co doping could further lower the kinetic energy barrier by promoting H–H bond formation on two adjacently adsorbed H_{ads}.

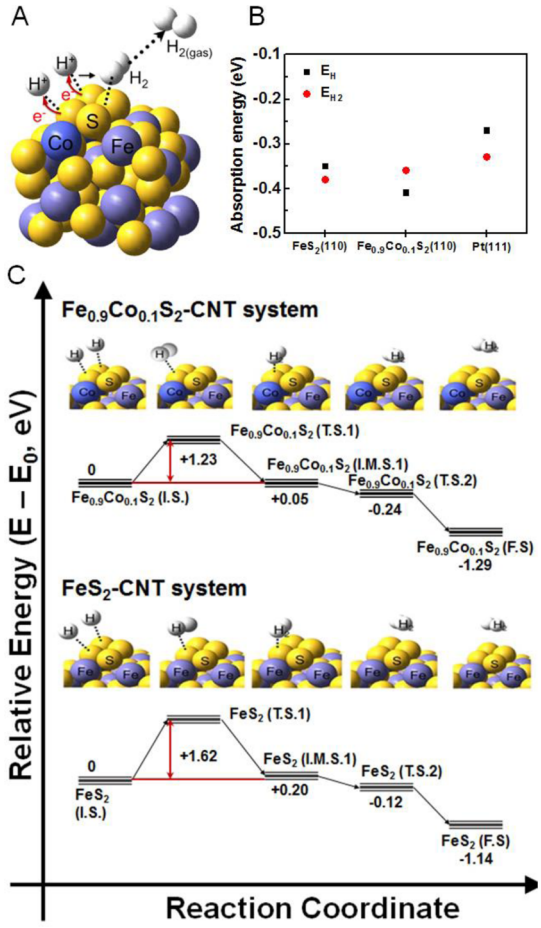

Figure 5. (A) Schematic reaction pathway of hydrogen evolution on sulfur atom of $Fe_{0.9}Co_{0.1}S_2$ edges in acid environment. (B) The adsorption energy of H atom and H_2 molecule on FeS_2 (110), $Fe_{0.9}Co_{0.1}S_2$ (110), and Pt (111) catalyst calculated by DFT simulation. (C) The kinetic energy barrier profiles of hydrogen evolution reaction on $Fe_{0.9}Co_{0.1}S_2$ (top) and FeS_2 (down) catalysts.

4. CONCLUSIONS

In summary, we have developed a scalable synthesis of $Fe_{0.9}Co_{0.1}S_2$ nanosheets–CNT hybrid catalysts via a facile solvothermal approach. With moderate Co doping ratio and excellent electrical coupling to the underlying carbon nanotube, the $Fe_{0.9}Co_{0.1}S_2$/CNT hybrid catalyst exhibited high HER activity with low overpotential of ~0.12 V (20 mA/cm^2 at a loading of 7 mg/cm^2), small Tafel slope of ~46 mV/decade and high long-term durability in acid solutions. According to DFT results, Co doping into FeS_2 catalyst reduced the energy barrier for transition state 1 (TS1) of hydrogen atom adsorption. The $Fe_{0.9}Co_{0.1}S_2$/CNT hybrid catalyst could be promising to replace precious metal catalysts for clean H_2 production in practical applications.

■ ASSOCIATED CONTENT

Supporting Information

Computational method, detailed synthesis method, SEM image, and EXAFS data of the hybrid catalysts. This material is available free of charge via the Internet at http://pubs.acs.org.

■ AUTHOR INFORMATION

Corresponding Authors

bjh@mail.ntust.edu.tw

DOI: 10.1021/ja511572q
J. Am. Chem. Soc. 2015, 137, 1587–1592

cjchen@ntnu.edu.tw
hdai@stanford.edu

Author Contributions

D.Y.W. and M.G. contributed equally to this work.

Notes

The authors declare no competing financial interest.

■ ACKNOWLEDGMENTS

This work was supported by a grant from Stanford GCEP, a Steinhart/Reed Award from the Stanford Precourt Institute for Energy and DOE.

■ REFERENCES

(1) Greeley, J.; Jaramillo, T. F.; Bonde, J.; Chorkendorff, I. B.; Norskov, J. K. *Nat. Mater.* **2006**, *5*, 909.
(2) (a) Gong, M.; Zhou, W.; Tsai, M.-C.; Zhou, J.; Guan, M.; Lin, M.-C.; Zhang, B.; Hu, Y.; Wang, D.-Y.; Yang, J.; Pennycook, S. J.; Hwang, B.-J.; Dai, H. *Nat. Commun.* **2014**, *5*, No. 4695. (b) Holladay, J. D.; Hu, J.; King, D. L.; Wang, Y. *Catal. Today* **2009**, *139*, 244.
(3) Walter, M. G.; Warren, E. L.; McKone, J. R.; Boettcher, S. W.; Mi, Q. X.; Santori, E. A.; Lewis, N. S. *Chem. Rev.* **2010**, *110*, 6446.
(4) Dresselhaus, M. S.; Thomas, I. L. *Nature* **2001**, *414*, 332.
(5) Norskov, J. K.; Bligaard, T.; Rossmeisl, J.; Christensen, C. H. *Nat. Chem.* **2009**, *1*, 37.
(6) Jaramillo, T. F.; Jorgensen, K. P.; Bonde, J.; Nielsen, J. H.; Horch, S.; Chorkendorff, I. *Science* **2007**, *317*, 100.
(7) Kibsgaard, J.; Chen, Z. B.; Reinecke, B. N.; Jaramillo, T. F. *Nat. Mater.* **2012**, *11*, 963.
(8) Voiry, D.; Yamaguchi, H.; Li, J. W.; Silva, R.; Alves, D. C. B.; Fujita, T.; Chen, M. W.; Asefa, T.; Shenoy, V. B.; Eda, G.; Chhowalla, M. *Nat. Mater.* **2013**, *12*, 850.
(9) Faber, M. S.; Jin, S. *Energy Environ. Sci.* **2014**, *7*, 3519.
(10) Faber, M. S.; Lukowski, M. A.; Ding, Q.; Kaiser, N. S.; Jin, S. *J. Phys. Chem. C* **2014**, *118*, 21347.
(11) Faber, M. S.; Dziedzic, R.; Lukowski, M. A.; Kaiser, N. S.; Ding, Q.; Jin, S. *J. Am. Chem. Soc.* **2014**, *136*, 10053.
(12) Sun, Y.; Liu, C.; Grauer, D. C.; Yano, J.; Long, J. R.; Yang, P.; Chang, C. J. *J. Am. Chem. Soc.* **2013**, *135*, 17699.
(13) Kong, D.; Cha, J. J.; Wang, H.; Lee, H. R.; Cui, Y. *Energy Environ. Sci.* **2013**, *6*, 3553.
(14) Chen, W. F.; Sasaki, K.; Ma, C.; Frenkel, A. I.; Marinkovic, N.; Muckerman, J. T.; Zhu, Y. M.; Adzic, R. R. *Angew. Chem., Int. Ed.* **2012**, *51*, 6131.
(15) Vrubel, H.; Hu, X. L. *Angew. Chem., Int. Ed.* **2012**, *51*, 12703.
(16) Popczun, E. J.; McKone, J. R.; Read, C. G.; Biacchi, A. J.; Wiltrout, A. M.; Lewis, N. S.; Schaak, R. E. *J. Am. Chem. Soc.* **2013**, *135*, 9267.
(17) Shima, S.; Pilak, O.; Vogt, S.; Schick, M.; Stagni, M. S.; Meyer-Klaucke, W.; Warkentin, E.; Thauer, R. K.; Ermler, U. *Science* **2008**, *321*, 572.
(18) Li, Y.; Wang, H.; Xie, L.; Liang, Y.; Hong, G.; Dai, H. *J. Am. Chem. Soc.* **2011**, *133*, 7296.
(19) Bonde, J.; Moses, P. G.; Jaramillo, T. F.; Norskov, J. K.; Chorkendorff, I. *Faraday Discuss.* **2008**, *140*, 219.
(20) Li, D. J.; Maiti, U. N.; Lim, J.; Choi, D. S.; Lee, W. J.; Oh, Y.; Lee, G. Y.; Kim, S. O. *Nano Lett.* **2014**, *14*, 1228.
(21) Liu, H. S.; Song, C. J.; Zhang, L.; Zhang, J. J.; Wang, H. J.; Wilkinson, D. P. *J. Power Sources* **2006**, *155*, 95.
(22) Stamenkovic, V. R.; Fowler, B.; Mun, B. S.; Wang, G. F.; Ross, P. N.; Lucas, C. A.; Markovic, N. M. *Science* **2007**, *315*, 493.
(23) Wang, D. Y.; Chou, H. L.; Lin, Y. C.; Lai, F. J.; Chen, C. H.; Lee, J. F.; Hwang, B. J.; Chen, C. C. *J. Am. Chem. Soc.* **2012**, *134*, 10011.
(24) Stamenkovic, V. R.; Mun, B. S.; Arenz, M.; Mayrhofer, K. J. J.; Lucas, C. A.; Wang, G. F.; Ross, P. N.; Markovic, N. M. *Nat. Mater.* **2007**, *6*, 241.
(25) Russell, A. E.; Rose, A. *Chem. Rev.* **2004**, *104*, 4613.
(26) Stamenkovic, V.; Mun, B. S.; Mayrhofer, K. J. J.; Ross, P. N.; Markovic, N. M.; Rossmeisl, J.; Greeley, J.; Norskov, J. K. *Angew. Chem., Int. Ed.* **2006**, *45*, 2897.
(27) Nørskov, J. K.; Bligaard, T.; Logadottir, A.; Kitchin, J. R.; Chen, J. G.; Pandelov, S.; Stimming, U. *J. Electrochem. Soc.* **2005**, *152*, J23.
(28) Hinnemann, B.; Moses, P. G.; Bonde, J.; Jorgensen, K. P.; Nielsen, J. H.; Horch, S.; Chorkendorff, I.; Norskov, J. K. *J. Am. Chem. Soc.* **2005**, *127*, 5308.
(29) Skulason, E.; Karlberg, G. S.; Rossmeisl, J.; Bligaard, T.; Greeley, J.; Jonsson, H.; Norskov, J. K. *Phys. Chem. Chem. Phys.* **2007**, *9*, 3241.
(30) Liang, D.; Caban-Acevedo, M.; Kaiser, N. S.; Jin, S. *Nano Lett.* **2014**, *14*, 6754.
(31) Wang, D. Y.; Jiang, Y. T.; Lin, C. C.; Li, S. S.; Wang, Y. T.; Chen, C. C.; Chen, C. W. *Adv. Mater.* **2012**, *24*, 3415.
(32) Liang, Y.; Li, Y.; Wang, H.; Dai, H. *J. Am. Chem. Soc.* **2013**, *135*, 2013.
(33) (a) Wang, H.; Dai, H. *Chem. Soc. Rev.* **2013**, *42*, 3088. (b) Gong, M.; Dai, H. *Nano Res.* **2015**, *8*, 23. (c) Li, J. Y.; Wang, G. X.; Wang, J.; Miao, S.; Wei, M. M.; Yang, F.; Yu, L.; Bao, X. H. *Nano Res.* **2014**, *7*, 1519. (d) Feng, J.; Liang, Y. Y.; Wang, H. L.; Li, Y. G.; Zhang, B.; Zhou, J. G.; Wang, J.; Regier, T.; Dai, H. J. *Nano Res.* **2012**, *5*, 718.
(34) Liang, Y.; Wang, H.; Diao, P.; Chang, W.; Hong, G.; Li, Y.; Gong, M.; Xie, L.; Zhou, J.; Wang, J.; Regier, T. Z.; Wei, F.; Dai, H. *J. Am. Chem. Soc.* **2012**, *134*, 15849.
(35) Li, Y.; Gong, M.; Liang, Y.; Feng, J.; Kim, J. E.; Wang, H.; Hong, G.; Zhang, B.; Dai, H. *Nat. Commun.* **2013**, *4*, 1805.
(36) Gong, M.; Li, Y.; Wang, H.; Liang, Y.; Wu, J. Z.; Zhou, J.; Wang, J.; Regier, T.; Wei, F.; Dai, H. *J. Am. Chem. Soc.* **2013**, *135*, 8452.
(37) Feng, J.; Liang, Y.; Wang, H.; Li, Y.; Zhang, B.; Zhou, J.; Wang, J.; Regier, T.; Dai, H. *Nano Res.* **2012**, *5*, 718.
(38) Hummers, W. S.; Offeman, R. E. *J. Am. Chem. Soc.* **1958**, *80*, 1339.
(39) O'Day, P. A.; Rivera, N.; Root, R.; Carroll, S. A. *Am. Mineral.* **2004**, *89*, 572.
(40) Kadono, T.; Kubota, T.; Hiromitsu, I.; Okamoto, Y. *Appl. Catal., A* **2006**, *312*, 125.
(41) Wang, H.; Kong, D.; Johanes, P.; Cha, J. J.; Zheng, G.; Yan, K.; Liu, N.; Cui, Y. *Nano Lett.* **2013**, *13*, 3426.
(42) Choi, C. L.; Feng, J.; Li, Y.; Wu, J.; Zak, A.; Tenne, R.; Dai, H. *Nano Res.* **2013**, *6*, 921.
(43) Lee, W. J.; Lee, J. M.; Kochuveedu, S. T.; Han, T. H.; Jeong, H. Y.; Park, M.; Yun, J. M.; Kwon, J.; No, K.; Kim, D. H.; Kim, S. O. *ACS Nano* **2012**, *6*, 935.
(44) Maiti, U. N.; Lee, W. J.; Lee, J. M.; Oh, Y.; Kim, J. Y.; Kim, J. E.; Shim, J.; Han, T. H.; Kim, S. O. *Adv. Mater.* **2014**, *26*, 40.
(45) Liang, Y. Y.; Li, Y. G.; Wang, H. L.; Zhou, J. G.; Wang, J.; Regier, T.; Dai, H. J. *Nat. Mater.* **2011**, *10*, 780.
(46) Fang, Y.-H.; Wei, G.-F.; Liu, Z.-P. *J. Phys. Chem. C* **2013**, *117*, 7669.

DOI: 10.1021/ja511572q
J. Am. Chem. Soc. 2015, 137, 1587−1592